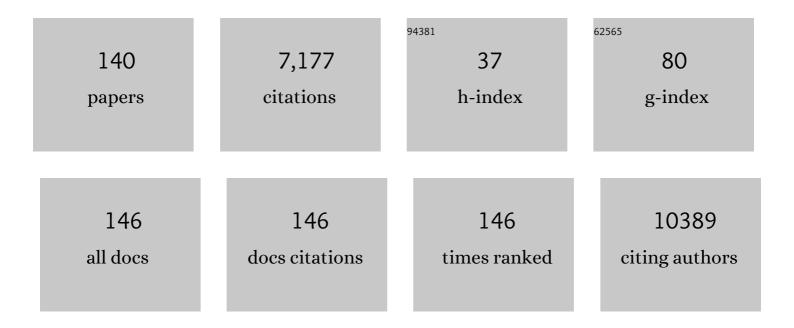
Aleksander Gurlo

List of Publications by Year in descending order

Source: https://exaly.com/author-pdf/979899/publications.pdf Version: 2024-02-01



ALEKSANDED CUDIO

#	Article	IF	CITATIONS
1	CrabNet for Explainable Deep Learning in Materials Science: Bridging the Gap Between Academia and Industry. Integrating Materials and Manufacturing Innovation, 2022, 11, 41-56.	1.2	3
2	Elucidating the role of earth alkaline doping in perovskite-based methane dry reforming catalysts. Catalysis Science and Technology, 2022, 12, 1229-1244.	2.1	6
3	Effect of <i>Fomes fomentarius</i> Cultivation Conditions on Its Adsorption Performance for Anionic and Cationic Dyes. ACS Omega, 2022, 7, 4158-4169.	1.6	9
4	Solar hydrogen generation using niobium-based photocatalysts: design strategies, progress, and challenges. Materials Today Energy, 2022, 24, 100936.	2.5	9
5	Review of space resources processing for Mars missions: Martian simulants, regolith bonding concepts and additive manufacturing. Open Ceramics, 2022, 9, 100216.	1.0	18
6	Ceramic Stereolithography of Bioactive Glasses: Influence of Resin Composition on Curing Behavior and Green Body Properties. Biomedicines, 2022, 10, 395.	1.4	9
7	Fabrication and characterization of porous mullite ceramics derived from fluoride-assisted Metakaolin-Al(OH)3 annealing for filtration applications. Open Ceramics, 2022, 9, 100240.	1.0	9
8	A comparison of syntheses approaches towards functional polycrystalline silicate ceramics. Open Ceramics, 2022, 9, 100241.	1.0	3
9	Stable anodes for lithium-ion batteries based on tin-containing silicon oxycarbonitride ceramic nanocomposites. Materials Today Energy, 2022, 26, 100989.	2.5	12
10	Atomic-Scale Insights into Nickel Exsolution on LaNiO ₃ Catalysts via <i>In Situ</i> Electron Microscopy. Journal of Physical Chemistry C, 2022, 126, 786-796.	1.5	14
11	Springback effect and structural features during the drying of silica aerogels tracked by in-situ synchrotron X-ray scattering. Scientific Reports, 2022, 12, 7537.	1.6	10
12	Steering the Methane Dry Reforming Reactivity of Ni/La ₂ O ₃ Catalysts by Controlled In Situ Decomposition of Doped La ₂ NiO ₄ Precursor Structures. ACS Catalysis, 2021, 11, 43-59.	5.5	38
13	Coaxial nanofibers of nickel/gadolinium oxide/nickel oxide as highly effective electrocatalysts for hydrogen evolution reaction. Journal of Colloid and Interface Science, 2021, 587, 457-466.	5.0	47
14	Steering the methanol steam reforming reactivity of intermetallic Cu–In compounds by redox activation: stability <i>vs.</i> formation of an intermetallic compound–oxide interface. Catalysis Science and Technology, 2021, 11, 5518-5533.	2.1	3
15	Silicon oxycarbonitride ceramic containing nickel nanoparticles: from design to catalytic application. Materials Advances, 2021, 2, 1715-1730.	2.6	8
16	Mechanistic in situ insights into the formation, structural and catalytic aspects of the La2NiO4 intermediate phase in the dry reforming of methane over Ni-based perovskite catalysts. Applied Catalysis A: General, 2021, 612, 117984.	2.2	16
17	Review on Polymeric, Inorganic, and Composite Materials for Air Filters: From Processing to Properties. Advanced Energy and Sustainability Research, 2021, 2, 2100005.	2.8	20
18	Silicate dielectric ceramics for millimetre wave applications. Journal of the European Ceramic Society, 2021, 41, 3879-3894.	2.8	43

#	Article	IF	CITATIONS
19	Polymer derived ceramic aerogels. Current Opinion in Solid State and Materials Science, 2021, 25, 100936.	5.6	19
20	Bispropylurea bridged polysilsesquioxane: A microporous MOF-like material for molecular recognition. Chemosphere, 2021, 276, 130181.	4.2	14
21	AIF3-assisted flux growth of mullite whiskers and their application in fabrication of porous mullite-alumina monoliths. Open Ceramics, 2021, 7, 100145.	1.0	6
22	Cu-Modified SrTiO ₃ Perovskites Toward Enhanced Water–Gas Shift Catalysis: A Combined Experimental and Computational Study. ACS Applied Energy Materials, 2021, 4, 452-461.	2.5	15
23	Extrusion-based additive manufacturing of fungal-based composite materials using the tinder fungus Fomes fomentarius. Fungal Biology and Biotechnology, 2021, 8, 21.	2.5	9
24	Fabrication of polymer-derived ceramics with hierarchical porosities by freeze casting assisted by thiol-ene click chemistry and HF etching. Journal of the European Ceramic Society, 2020, 40, 315-323.	2.8	10
25	Improving the physicochemical properties of Y zeolite for catalytic cracking of heavy oil via sequential steam-alkali-acid treatments. Microporous and Mesoporous Materials, 2020, 294, 109854.	2.2	27
26	On-chip assembly of 3D graphene-based aerogels for chemiresistive gas sensing. Chemical Communications, 2020, 56, 450-453.	2.2	39
27	In Situ-Determined Catalytically Active State of LaNiO ₃ in Methane Dry Reforming. ACS Catalysis, 2020, 10, 1102-1112.	5.5	55
28	Carbide-Modified Pd on ZrO2 as Active Phase for CO2-Reforming of Methane—A Model Phase Boundary Approach. Catalysts, 2020, 10, 1000.	1.6	14
29	Low-temperature fluoride-assisted synthesis of mullite whiskers. RSC Advances, 2020, 10, 31180-31186.	1.7	12
30	Polymer-Derived SiOC Integrated with a Graphene Aerogel As a Highly Stable Li-Ion Battery Anode. ACS Applied Materials & Interfaces, 2020, 12, 46045-46056.	4.0	66
31	Machine Learning for Materials Scientists: An Introductory Guide toward Best Practices. Chemistry of Materials, 2020, 32, 4954-4965.	3.2	224
32	Fabrication and Characterization of Ice Templated Membrane Supports from Portland Cement. Membranes, 2020, 10, 93.	1.4	9
33	Clay in situ resource utilization with Mars global simulant slurries for additive manufacturing and traditional shaping of unfired green bodies. Acta Astronautica, 2020, 174, 241-253.	1.7	23
34	Freeze Casting: From Lowâ€Dimensional Building Blocks to Aligned Porous Structures—A Review of Novel Materials, Methods, and Applications. Advanced Materials, 2020, 32, e1907176.	11.1	404
35	Azo dye adsorption on an industrial waste-transformed hydroxyapatite adsorbent: Kinetics, isotherms, mechanism and regeneration studies. Journal of Environmental Chemical Engineering, 2020, 8, 103807.	3.3	93
36	Metal-containing ceramic nanocomposites synthesized from metal acetates and polysilazane. Open Ceramics, 2020, 1, 100001.	1.0	15

#	Article	IF	CITATIONS
37	Zirconium Oxycarbide: A Highly Stable Catalyst Material for Electrochemical Energy Conversion. ChemPhysChem, 2019, 20, 3067-3073.	1.0	6
38	Revealing the Mechanism of Multiwalled Carbon Nanotube Growth on Supported Nickel Nanoparticles by in Situ Synchrotron X-ray Diffraction, Density Functional Theory, and Molecular Dynamics Simulations. ACS Catalysis, 2019, 9, 6999-7011.	5.5	36
39	Influence of Composition on Mechanical Properties of Additively Manufactured Composites Reinforced with Endless Carbon Fibers. Key Engineering Materials, 2019, 809, 335-340.	0.4	4
40	Ceria-Based Dual-Phase Membranes for High-Temperature Carbon Dioxide Separation: Effect of Iron Doping and Pore Generation with MgO Template. Membranes, 2019, 9, 108.	1.4	8
41	Materials and Applications for Low-Cost Ceramic Membranes. Membranes, 2019, 9, 105.	1.4	106
42	Treading in the Limited Stability Regime of Lanthanum Strontium Ferrite — Reduction, Phase Change and Exsolution. ECS Transactions, 2019, 91, 1771-1781.	0.3	4
43	Crystallographic and electronic evolution of lanthanum strontium ferrite (La _{0.6} Sr _{0.4} FeO _{3â^îr}) thin film and bulk model systems during iron exsolution. Physical Chemistry Chemical Physics, 2019, 21, 3781-3794.	1.3	18
44	High specific surface area ordered mesoporous silica COK-12 with tailored pore size. Microporous and Mesoporous Materials, 2019, 280, 133-143.	2.2	18
45	On the structural stability of crystalline ceria phases in undoped and acceptor-doped ceria materials under <i>in situ</i> reduction conditions. CrystEngComm, 2019, 21, 145-154.	1.3	32
46	Evaluating porous polylactide-co-glycolide/bioactive glass composite microsphere powders for laser sintering of scaffolds. Powder Technology, 2019, 354, 289-300.	2.1	10
47	Real-time direct transmission electron microscopy imaging of phase and morphology transformation from solid indium oxide hydroxide to hollow corundum-type indium oxide nanocrystallites. Nanoscale, 2019, 11, 12242-12249.	2.8	4
48	Reactive metal-support interaction in the Cu-In ₂ O ₃ system: intermetallic compound formation and its consequences for CO ₂ -selective methanol steam reforming. Science and Technology of Advanced Materials, 2019, 20, 356-366.	2.8	26
49	High-temperature structure or <mmi:math xmlns:mml="http://www.w3.org/1998/Math/MathML"> <mml:mrow> <mml:msub> <mml:mi>Co</mml:mi> <mml: mathvariant="normal">O <mml:mn>4</mml:mn> </mml: </mml:msub> </mml:mrow> : Understanding spinel inversion using <i>in situ</i></mmi:math 	mn>31.1	ml:mn> 11
50	8, 2019, 99, Additive manufacturing of ceramics from preceramic polymers: A versatile stereolithographic approach assisted by thiol-ene click chemistry. Additive Manufacturing, 2019, 27, 80-90.	1.7	98
51	Grafting and stabilization of ordered mesoporous silica COK-12 with graphene oxide for enhanced removal of methylene blue. RSC Advances, 2019, 9, 36271-36284.	1.7	19
52	Functionalization of MCM-41 with titanium oxynitride deposited via PECVD for enhanced removal of methylene blue. Journal of Molecular Liquids, 2019, 274, 505-515.	2.3	37
53	In-vitro investigation of graphene oxide reinforced bioactive glass ceramics composites. Journal of Non-Crystalline Solids, 2019, 505, 122-130.	1.5	18
54	Investigation of the role of the Na2WO4/Mn/SiO2 catalyst composition in the oxidative coupling of methane by chemical looping experiments. Journal of Catalysis, 2018, 360, 102-117.	3.1	76

#	Article	IF	CITATIONS
55	Bilayer graded Al/B ₄ C/rice husk ash composite: Wettability behavior, thermo-mechanical, and electrical properties. Journal of Composite Materials, 2018, 52, 3745-3758.	1.2	27
56	Transmission <i>in situ</i> and <i>operando</i> high temperature X-ray powder diffraction in variable gaseous environments. Review of Scientific Instruments, 2018, 89, 033904.	0.6	33
57	Ferrimagnetism in manganese-rich gallium and aluminium spinels due to mixed valence Mn ²⁺ –Mn ³⁺ states. Dalton Transactions, 2018, 47, 2727-2738.	1.6	15
58	Delayed release of chemokine CCL25 with bioresorbable microparticles for mobilization of human mesenchymal stem cells. Acta Biomaterialia, 2018, 69, 290-300.	4.1	8
59	Structural investigations of La _{0.6} Sr _{0.4} FeO _{3â~Î} under reducing conditions: kinetic and thermodynamic limitations for phase transformations and iron exsolution phenomena. RSC Advances, 2018, 8, 3120-3131.	1.7	37
60	Tailoring of ordered mesoporous silica COK-12: Room temperature synthesis of mesocellular foam and multilamellar vesicles. Microporous and Mesoporous Materials, 2018, 267, 142-149.	2.2	22
61	Hydrothermal synthesis of nanocrystalline hydroxyapatite from phosphogypsum waste. Journal of Environmental Chemical Engineering, 2018, 6, 1347-1352.	3.3	54
62	Surface modification of rice-husk ash (RHA) by Si3N4 coating to promote its wetting by Al-Mg-Si alloys. Materials Chemistry and Physics, 2018, 203, 223-234.	2.0	17
63	Batch and continuous synthesis upscaling of powder and monolithic ordered mesoporous silica COK-12. Microporous and Mesoporous Materials, 2018, 256, 102-110.	2.2	17
64	Towards the colonization of Mars by in-situ resource utilization: Slip cast ceramics from Martian soil simulant. PLoS ONE, 2018, 13, e0204025.	1.1	21
65	Zirconiumâ€Assisted Activation of Palladium To Boost Syngas Production by Methane Dry Reforming. Angewandte Chemie - International Edition, 2018, 57, 14613-14618.	7.2	44
66	Revised model for thermopower and site inversion in <mml:math xmlns:mml="http://www.w3.org/1998/Math/MathML"><mml:mrow><mml:msub><mml:mi>Co</mml:mi><mml:r mathvariant="normal">O<mml:mn>4</mml:mn></mml:r </mml:msub></mml:mrow> spinel. Physical Review B, 2018, 98, .</mml:math 	nn>31.1	nl:mu>
67	Hydrogen reduction and metal-support interaction in a metastable metal-oxide system: Pd on rhombohedral In2O3. Journal of Solid State Chemistry, 2018, 266, 93-99.	1.4	11
68	Surface Carbon as a Reactive Intermediate in Dry Reforming of Methane to Syngas on a 5% Ni/MnO Catalyst. ACS Catalysis, 2018, 8, 8739-8750.	5.5	60
69	H2 reduction of Gd- and Sm-doped ceria compared to pure CeO2 at high temperatures: effect on structure, oxygen nonstoichiometry, hydrogen solubility and hydroxyl chemistry. Physical Chemistry Chemical Physics, 2018, 20, 22099-22113.	1.3	12
70	Formation of Pd-Ce intermetallic compounds by reductive metal-support interaction. Journal of Solid State Chemistry, 2018, 265, 176-183.	1.4	3
71	Scaled-up solvothermal synthesis of nanosized metastable indium oxyhydroxide (InOOH) and corundum-type rhombohedral indium oxide (rh-In ₂ O ₃). Zeitschrift Fur Kristallographie - Crystalline Materials, 2017, 232, 129-140.	0.4	9
72	Removal of cationic and anionic textile dyes with Moroccan natural phosphate. Journal of Environmental Chemical Engineering, 2017, 5, 2189-2199.	3.3	28

#	Article	IF	CITATIONS
73	Response of Gallium Nitride Chemiresistors to Carbon Monoxide is Due to Oxygen Contamination. ACS Sensors, 2017, 2, 713-717.	4.0	13
74	Manufacturing and Characterization of Highly Porous Bioactive Glass Composite Scaffolds Using Unidirectional Freeze Casting. Advanced Engineering Materials, 2017, 19, 1700129.	1.6	10
75	Surface chemistry of pure tetragonal ZrO ₂ and gas-phase dependence of the tetragonal-to-monoclinic ZrO ₂ transformation. Dalton Transactions, 2017, 46, 4554-4570.	1.6	31
76	Electrochemical study of NiO nanosheets: toward the understanding of capacity fading. Journal of Materials Science, 2017, 52, 6498-6505.	1.7	8
77	Eco-fabrication of hierarchical porous silica monoliths by ice-templating of rice husk ash. Green Chemistry, 2017, 19, 188-195.	4.6	66
78	Engaging the flux-grown La1â^'Sr Fe1â^'Ti O3 crystals in visible-light-driven photocatalytic hydrogen generation. International Journal of Hydrogen Energy, 2017, 42, 27024-27033.	3.8	14
79	Iron Exsolution Phenomena in Lanthanum Strontium Ferrite SOFC Anodes. ECS Transactions, 2017, 78, 1327-1341.	0.3	5
80	Elucidating the impact of A-site cation change on photocatalytic H ₂ and O ₂ evolution activities of perovskite-type LnTaON ₂ (Ln = La and Pr). Physical Chemistry Chemical Physics, 2017, 19, 22210-22220.	1.3	44
81	Surface chemistry and stability of metastable corundum-type In ₂ O ₃ . Physical Chemistry Chemical Physics, 2017, 19, 19407-19419.	1.3	13
82	Macroporous polymer-derived SiO2/SiOC monoliths freeze-cast from polysiloxane and amorphous silica derived from rice husk. Journal of the European Ceramic Society, 2017, 37, 4809-4820.	2.8	51
83	Metastable Corundum-Type In ₂ O ₃ : Phase Stability, Reduction Properties, and Catalytic Characterization. Journal of Physical Chemistry C, 2016, 120, 15272-15281.	1.5	11
84	Hydrate Networks under Mechanical Stress - A Case Study for Co3(PO4)2·8H2O. European Journal of Inorganic Chemistry, 2016, 2016, 2072-2081.	1.0	15
85	Mechanism of Gas Separation through Amorphous Silicon Oxycarbide Membranes. Advanced Engineering Materials, 2016, 18, 721-727.	1.6	14
86	The Thermal Conductivity of Polymerâ€Derived Amorphous Si–O–C Compounds and Nanoâ€Composites. Journal of the American Ceramic Society, 2016, 99, 281-285.	1.9	44
87	Fabrication of cellular and lamellar LiFePO ₄ /C Cathodes for Li-ion batteries by unidirectional freeze-casting method. Journal of the Ceramic Society of Japan, 2016, 124, 1067-1071.	0.5	15
88	The contrasting effect of the Ta/Nb ratio in (111)-layered B-site deficient hexagonal perovskite Ba ₅ Nb _{4â^x} Ta _x O ₁₅ crystals on visible-light-induced photocatalytic water oxidation activity of their oxynitride derivatives. Dalton Transactions, 2016, 45, 12559-12568.	1.6	24
89	Ferroelectric InMnO3: Growth of single crystals, structure and high-temperature phase transitions. Journal of Solid State Chemistry, 2016, 241, 54-63.	1.4	15
90	Silicon oxycarbonitrides synthesized by ammonia-assisted thermolysis route from polymers: A total X-ray scattering, solid-state NMR, and TEM structural study. Journal of the European Ceramic Society, 2016, 36, 979-989.	2.8	14

#	Article	IF	CITATIONS
91	New Dion–Jacobson Phase Three-Layer Perovskite CsBa ₂ Ta ₃ O ₁₀ and Its Conversion to Nitrided Ba ₂ Ta ₃ O ₁₀ Nanosheets via a Nitridation–Protonation–Intercalation–Exfoliation Route for Water Splitting. Crystal Growth and Design, 2016, 16, 2302-2308.	1.4	47
92	Ultramicroporous silicon nitride ceramics for CO ₂ capture. Journal of Materials Research, 2015, 30, 2958-2966.	1.2	11
93	Perovskiteâ€ŧype Solid Solution SrMo _{1–<i>x</i>} W <i>_x</i> (O, N) ₃ Oxynitrides: Synthesis, Structure, and Magnetic Properties. Zeitschrift Fur Anorganische Und Allgemeine Chemie, 2015, 641, 1533-1539.	0.6	5
94	NH ₃ -assisted synthesis of microporous silicon oxycarbonitride ceramics from preceramic polymers: a combined N ₂ and CO ₂ adsorption and small angle X-ray scattering study. Journal of Materials Chemistry A, 2015, 3, 805-818.	5.2	41
95	Synthesis and rapid sintering of dense SrA(O,N)3 (A=Mo, W) oxynitride ceramics. Journal of the European Ceramic Society, 2015, 35, 3273-3281.	2.8	3
96	Compressibility and structural stability of spinel-type MnIn2O4. Journal of Solid State Chemistry, 2015, 230, 301-308.	1.4	13
97	A study on the thermal conversion of scheelite-type ABO ₄ into perovskite-type AB(O,N) ₃ . Dalton Transactions, 2015, 44, 8238-8246.	1.6	21
98	Kinetic control in the synthesis of metastable polymorphs: Bixbyite-to-Rh2O3(II)-to-corundum transition in In2O3. Journal of Solid State Chemistry, 2015, 229, 278-286.	1.4	9
99	In situ formation of tungsten oxycarbide, tungsten carbide and tungsten nitride nanoparticles in micro- and mesoporous polymer-derived ceramics. Journal of Materials Chemistry A, 2014, 2, 10454.	5.2	26
100	Hybrid Organotin and Tin Oxide-based Thin Films Processed from Alkynylorganotins: Synthesis, Characterization, and Gas Sensing Properties ACS Applied Materials & Interfaces, 2014, 6, 17093-17101.	4.0	28
101	High-Temperature Stability and Saturation Magnetization of Superparamagnetic Nickel Nanoparticles in Microporous Polysilazane-Derived Ceramics and their Gas Permeation Properties. ACS Applied Materials & Interfaces, 2014, 6, 12270-12278.	4.0	26
102	Fabrication of nitrogen-doped TiO2 monolith with well-defined macroporous and bicrystalline framework and its photocatalytic performance under visible light. Journal of the European Ceramic Society, 2014, 34, 809-816.	2.8	35
103	Monitoring Gas Sensors at Work: Operando Raman–FTIR Study of Ethanol Detection by Indium Oxide. Angewandte Chemie - International Edition, 2013, 52, 3607-3610.	7.2	55
104	Theoretical study on copper's energetics and magnetism in TiO2 polymorphs. Journal of Applied Physics, 2013, 113, .	1.1	48
105	In situ high pressure high temperature experiments in multi-anvil assemblies with bixbyite-type In2 O3 and synthesis of corundum-type and orthorhombic In2 O3 polymorphs. High Pressure Research, 2013, 33, 697-711.	0.4	16
106	Insights into the Mechanism of Gas Sensor Operation. , 2013, , 3-34.		5
107	Visible Light Photocatalysis with c-WO _{3–<i>x</i>} /WO ₃ ×H ₂ O Nanoheterostructures In Situ Formed in Mesoporous Polycarbosilane-Siloxane Polymer. Journal of the American Chemical Society, 2013, 135, 4467-4475.	6.6	150
108	Orthorhombic In ₂ O ₃ : A Metastable Polymorph of Indium Sesquioxide. Angewandte Chemie - International Edition, 2013, 52, 6531-6535.	7.2	42

#	Article	IF	CITATIONS
109	Orthorhombisches In ₂ O ₃ – ein metastabiles Indiumsesquioxid―Polymorph. Angewandte Chemie, 2013, 125, 6659-6663.	1.6	2
110	Phase segregation in Mn-doped In2O3: in situ high-pressure high-temperature synchrotron studies in multi-anvil assemblies. RSC Advances, 2013, 3, 5357.	1.7	4
111	Indium hydroxide to oxide decomposition observed in one nanocrystal during in situ transmission electron microscopy studies. Journal of Solid State Chemistry, 2013, 198, 364-370.	1.4	12
112	Can we predict the formability of perovskite oxynitrides from tolerance and octahedral factors?. Journal of Materials Chemistry A, 2013, 1, 12239.	5.2	61
113	Inkjetâ€Printed Nanoscaled CuO for Miniaturized Gasâ€Sensing Devices. European Journal of Inorganic Chemistry, 2013, 2013, 1481-1487.	1.0	4
114	<i>trans</i> -Bis(acetato-lº <i>O</i>)bis(2-aminoethanol-lº ² <i>N</i> , <i>O</i>)nickel(II). Acta Crystallographica Section E: Structure Reports Online, 2012, 68, m567-m568.	0.2	4
115	Low temperature synthesis of nanocrystalline MnIn2O4 spinel. Dalton Transactions, 2012, 41, 3374.	1.6	15
116	Nanoscaled tin dioxide films processed from organotin-based hybrid materials: an organometallic route toward metal oxide gas sensors. Nanoscale, 2012, 4, 6806.	2.8	40
117	Ab initio study of phase stability in doped TiO2. Computational Mechanics, 2012, 50, 185-194.	2.2	78
118	Enhanced n-type thermopower in distortion-free LiMn2O4. Journal of Materials Chemistry, 2012, 22, 4631.	6.7	15
119	Template-free synthesis of polymer-derived mesoporous SiOC/TiO2 and SiOC/N-doped TiO2 ceramic composites for application in the removal of organic dyes from contaminated water. Applied Catalysis B: Environmental, 2012, 115-116, 303-313.	10.8	63
120	Thermal decomposition of carbon-rich polymer-derived silicon carbonitrides leading to ceramics with high specific surface area and tunable micro- and mesoporosity. Journal of the European Ceramic Society, 2012, 32, 477-484.	2.8	64
121	Low-temperature H2sensing in self-assembled organotin thin films. Chemical Communications, 2011, 47, 1464-1466.	2.2	20
122	A molecular approach to Cu doped ZnO nanorods with tunable dopant content. Dalton Transactions, 2011, 40, 4307.	1.6	37
123	Nanoporous Silicon Oxycarbonitride Ceramics Derived from Polysilazanes In situ Modified with Nickel Nanoparticles. Chemistry of Materials, 2011, 23, 4112-4123.	3.2	78
124	Nanosensors: towards morphological control of gas sensing activity. SnO ₂ , In ₂ O ₃ , ZnO and WO ₃ case studies. Nanoscale, 2011, 3, 154-165.	2.8	399
125	Review of the anatase to rutile phase transformation. Journal of Materials Science, 2011, 46, 855-874.	1.7	2,530
126	Highâ€Sensitivity Hydrogen Detection: Hydrogenâ€Induced Swelling of Multiple Cracked Palladium Films on Compliant Substrates. Angewandte Chemie - International Edition, 2011, 50, 10130-10132.	7.2	25

Aleksander Gurlo

#	Article	IF	CITATIONS
127	Active Metal Electrode–Oxide Interface in Gas Sensor Operation Probed by In Situ and Timeâ€Resolved Xâ€Ray Spectroscopy. ChemPhysChem, 2010, 11, 79-82.	1.0	12
128	Multilayer Amorphous‧iâ€Bâ€Câ€N/γâ€Al ₂ O ₃ /αâ€Al ₂ O ₃ Membranes for Hydrogen Purification. Advanced Engineering Materials, 2010, 12, 522-528.	1.6	32
129	Synthesemethoden für keramische Materialien. Hochtechnologiewerkstoffe. Chemie in Unserer Zeit, 2010, 44, 208-227.	0.1	8
130	Structural Stability of Highâ€Pressure Polymorphs in In ₂ O ₃ Nanocrystals: Evidence of Stressâ€Induced Transition?. Angewandte Chemie - International Edition, 2010, 49, 5610-5612.	7.2	31
131	Nanosensors: Does Crystal Shape Matter?. Small, 2010, 6, 2077-2079.	5.2	52
132	Sensing in harsh conditions: How to protect SnO <inf>2</inf> sensing layer. , 2010, , .		0
133	Pressure-Induced Decomposition of Indium Hydroxide. Journal of the American Chemical Society, 2010, 132, 12674-12678.	6.6	9
134	Molecular based, chimie douce approach to 0D and 1D indium oxide nanostructures. Evaluation of their sensing properties towards CO and H2. Journal of Materials Chemistry, 2010, 20, 8311.	6.7	46
135	Synthesis and sensoric response of ZnO decorated carbon nanotubes. Journal of Materials Chemistry, 2009, 19, 5039.	6.7	76
136	Surfactant-free self-assembly route to hollow In2O3 microspheres. Chemical Communications, 2009, , 2747.	2.2	24
137	Metastability of Corundumâ€Type In ₂ O ₃ . Chemistry - A European Journal, 2008, 14, 3306-3310.	1.7	77
138	Highâ€pressure highâ€temperature synthesis of Rh ₂ O ₃ â€llâ€type In ₂ O ₃ polymorph. Physica Status Solidi - Rapid Research Letters, 2008, 2, 269-271.	1.2	32
139	Nanocubes or Nanorhombohedra? Unusual Crystal Shapes of Corundum-Type Indium Oxide. Journal of Physical Chemistry C, 2008, 112, 9209-9213.	1.5	46
140	Shape-, size- and phase-controlled indium oxide for gas sensing. , 2008, , .		1

Shape-, size- and phase-controlled indium oxide for gas sensing. , 2008, , . 140